



Sewer chamber design under critical conditions using computational fluid dynamics (CFD)

Tyler Tsuchida^{a,b}, Joshua Lelemia Irvine^a, Siufung Tang^a, Jamie Nishikawa^b,
Leighton Lum^b, Albert S. Kim^{a,*}

^aCivil and Environmental Engineering, University of Hawaii at Manoa, 2540 Dole Street Holmes 383, Honolulu, Hawaii 96822, USA, Tel. +1 808 956 3718; Fax: +1 808 956 5014; email: albertsk@hawaii.edu (A.S. Kim)

^bR. M. Towill Corporation, 2024 North King Street, Honolulu, Hawaii 96819, USA

Received 24 January 2018; Accepted 2 February 2018

ABSTRACT

Transient sewage flow patterns inside a utility chamber are studied using open source computational fluid dynamics software, OpenFOAM. The solver used is based on Reynolds-averaged Navier–Stokes equations with $\kappa - \epsilon$ turbulence model. We found that there are two distinct flow regimes based on the inflow rate. For a low inflow rate, the sewage level does not exceed the outlet pipe, and a steady state is reached within a minute. For a high inflow rate, the tantalizing phenomenon is observed such that the sewage level periodically moves up and down passing the top of the outlet pipe. In this case, a steady state is intrinsically absent, and the sewage level continuously fluctuates for a long time. A chamber overflow occurs with a small outlet diameter and a fast inflow rate. Using Scotch algorithm, parallel computation of an OpenFOAM solver, interFoam, has been efficiently conducted within a reasonable amount of time.

Keywords: Computational fluid dynamics; OpenFOAM; Sewer design; Manhole flow; Urban runoff

1. Introduction

Storms and heavy rains often cause deleterious urban flows in short periods of time and therefore become critical issues in maintaining sustainable urban infrastructure. During storm events, a fraction of initial runoffs is captured by porous natural surfaces such as grasses/lawn fields, detention ponds, and catchment systems. Sewage systems collect waters and redirect the collected sewage to water/wastewater treatment plants or natural water bodies (such as wetlands, lakes, and rivers). In tropical regions where cities are close to beaches, direct runoffs to the ocean trigger immediate non-point source pollution, and frequent unavailability of beaches impairs the tourism industry.

Utility holes (often called utility chambers or manholes) are installed for human inspection and maintenance along

the underground sewer pipelines. These chambers are expected to release hydraulic pressure and stabilize sewage flows under various hydrological conditions. Driving forces of the sewage flows are the hydraulic pressure and gravitation. Solid debris in the sewage flow often causes clogging problems in underground pipe systems, which can initiate reverse flow or spillover from the utility chambers. The water level of sewage flow often varies with time from its initial state. The fluctuating water–air interfaces contribute to mass transfer from sewage to air inside sewer chambers and therefore often generate unpleasant odor propagation to the atmosphere. Even though utility holes are designed for extreme hydrological scenarios, it is generally difficult to predict the overflow occurrence in large-scale hydrological events.

Several researchers used computational fluid dynamics (CFD) to study flow patterns and pressure distribution in underground pipelines and chambers. Iatan et al. [1] used commercial CFD software FLUENT to investigate open channel flow on a rough surface consisting of (ideal) hemispheres.

* Corresponding author.

They analyzed velocity, vorticity, and shear stress transport (SST) in turbulence regimes using an SST $k - \omega$ model [2], and rigorously studied effects of surface roughness on the SST. Their approach was, however, limited to the rough wall boundary region consisting of hemispheres. Hydraulic pressure applied on sewage flow upstream not only accelerates the flow speed along the pipe but also causes air circulation in the chamber, generating odor emission risk to the atmosphere. Edwini-Bonsu and Steffler used FEMLAB programming language embedded in MATLAB to calculate the ventilation rates in slanted sewer conduits [3]. The effect of interfacial drag of waste water is conceptually viewed as a Couette flow to describe the stable distribution of the air region above the water level. They used the Reynolds-averaged Navier–Stokes (RANS) equations [4] for an incompressible fluid, assuming the flow is fully developed in a steady state is already reached. Their approach is, however, unable to investigate transient behaviors of sewer flows, which primarily affect the air flow patterns above the sewage level.

Gullies and swales are human-made structures to collect large quantities of runoff water and carry the water to drain systems. CFD simulations of the water and air in the hydraulic systems can provide fundamental insight of mass and momentum exchanges between the two phases. As initial studies using CFD, Galambos [5] and Djordjević et al. [6] used OpenFOAM to model a UK gully-manhole system with qualitative verification. Leandro et al. [7] also used OpenFOAM to model water flow in a drainage system and reverse flows inside a gully. Due to the heavy computational load, real flows in the three-dimensional (3D) gully were simulated on a laterally averaged 2D plane. To compare the CFD simulations with experimental data, they calibrated critical parameters of a solver due to the irregular gully shape. In reality, gullies rarely have consistent profiles across long irregular stations and efficiency of CFD modeling is subjected to flow patterns along diverse gradients. Leandro et al.'s study indicates the difficulties of CFD modeling because of geometrical complexities and parametric calibration. These bottlenecks can be overcome by employing calibration-free solvers, which can be run fast in parallel computation using many computer cores. Previously, CFD modeling has been applied to specifically simulate the flow of dissolved solutes in a utility chamber under surcharged conditions [8]. In their study, Lau et al. [8] simulated stream flow in a chamber and investigated the particle distribution profile throughout the system. They additionally used cumulative retention time distributions to study effects of a hydraulic regime on solute transport processes. Even though these studies used the rigorous CFD for fluid flow in utility holes, the approaches were limited to 2D steady states. To the best of our knowledge, the transient 3D CFD simulations for two phases (water and air) in sewer systems are rare in the literature due to the heavy computational load.

The previous studies focused on hydraulic phenomena of utility chambers and influence of sewage flow on air ventilation in the steady state. The steady sewage level in the pipeline changes with hydrological conditions. In a dry period, the pipelines are partially filled with sewer water, but in a heavy precipitation period, sewage flow is similar to gravity-driven pipe flow. Dynamic changes in the inflow rate to the utility chamber noticeably influence the undesired hydraulic phenomena such as overflows as correlated to reverse flows

in the chamber pipeline systems. In reality, sewage flows in the underground utility chamber must be characterized as transient 3D open flows. To the best of our knowledge, past CFD studies paid much more attention to steady-state fluid flow passing utility holes, although transient fluid dynamics is the actual physical phenomena for sustainable designs.

The present work is based on a remodeling design project of a partial sewer system in Kaneohe, Hawaii. Most engineering and scientific research work begins with a specific hypothesis, which must be revised and modified until results confirm the underlying assumptions. Validation of the research output is often based on the reproducibility of experimental observation. Experimental data are often explained using fundamental theories, which can readily explain the observed phenomena. The theories should be able to further predict possible phenomenological scenarios to search for better or optimal performance. In addition to these two conventional methods, computer simulations became the third method about a half-century ago [9]. For multi-physics problems of complex systems, (theoretical) analytic solutions are formidable so that numerical approaches and computer simulations are sought to provide system-specific, accurate results. Recent developments in excellent software programs and computer hardware for fast parallel computing opened a new era of computer simulations for scientific discovery in addition to the standard validation of experimental observations. When scientific disciplines use theories based on well-accepted governing equations for specific phenomena, it implicitly approves results with physical meanings by properly solving the governing equations. Input, initial and boundary conditions should be physically meaningful and so do not violate the underlying sciences. Upon acceptance of this assumption, the modern trend of computational research exceeds the experimental validation and pursues reasonable discoveries by super-computing (<http://www.scidac.gov/>). The present study aims to identify the inflow conditions that cause specific flow behaviors in the utility chamber using OpenFOAM, an open-source CFD tool. The chamber is not yet built but still in the design phase. In-depth investigation of these phenomena is, in our opinion, a critical component for future civil engineering research, especially in the applied hydraulics discipline that requires more micro-scale analysis far from the steady-state assumption.

The present paper is, to the best of our knowledge, one of a few research papers that solved an engineering problem of applied hydraulics in an unsteady phase. Most of the hydraulic engineering design assumes steady states, which is, in our opinion, a forceful restriction to simplify the large-scale phenomena at the level of solvable applied mathematics. Reproducibility-based hydraulic research may require a lot of dollars, if it is forced, because a civil design is often for a unique purpose, to use large sizes. Duplication of hydraulic systems from one place to other places does not always guarantee a successful operation and optimal performance. Research on transient hydraulic phenomena is scarce in literature because it is challenging to verify and reproduce research outputs within a short period. In this case, we believe that computational engineering research, firmly based on fundamental sciences, should play a much more active role as the current civil designs pursue long-term sustainability.

The background and scope of the present study are as follows. The transition utility chamber was a part of a new

sewer design project to comply with the Consent Decree, an agreement between the Environmental Protection Agency, the State of Hawaii, and City and County of Honolulu. To achieve compliance, this project would construct a new sewer system that conveys increased wastewater flows expected in the future and minimize the probability of sewage overflow and spills. The project will decommission pipes delivering pressurized sewage flows to the existing force main sewer system, and construct a new gravity sewer system with external pumping options. System components to be built include utility chambers and 18-in (0.457 m) diameter sewer pipes of approximately 3,650 linear feet (1,112.5 m) long. Due to the topography of the existing sewer, however, not all of the force main system could be converted to a gravity flow system so a transition utility chamber was required. Due to the unique design requirements and constraints such as location, depth, width, and incoming flows, the project designers sought the aid of CFD modeling to investigate and visualize the interaction between the design structure and anticipated flows.

In this vein, we are specifically interested in overflow and spillover conditions of a utility chamber of specific geometry. Given the initial water level inside the utility chamber, if the inflow rate is low, then the chamber systems will reach a steady state in a short amount of time. Otherwise, sewage fluid will accumulate inside the chamber and initiate spillover to the street level. In our opinion, CFD studies on sewer systems should deal with the transient behavior of fluid flows since steady states barely occur in reality.

We use an open source CFD package, OpenFOAM, to study transient behavior of sewage flow inside a utility chamber, connected to inlet and outlet pipes of different diameters. In past decades, hydraulic CFD research has been limited in the literature because transient 3D simulations require enormous computational resources. Also, access to reliable open source CFD solvers was limited. We used OpenFOAM, of which performance and accuracy are known to be as good as commercial CFD software [10,11]. Some of our recent CFD work for filtration systems can be found elsewhere [12,13,14]. Here, we used two mainframe supercomputers to run our parallel hydraulic simulations, consisting of many computational cores. To the best of our knowledge, the present work is one of the rare studies that use OpenFOAM in a parallel mode to solve transient fluid flow and pressure distribution inside utility chambers. In the following sections, we will explain how to set up OpenFOAM cases including mesh generation and setting up initial conditions (ICs) and boundary conditions (BCs) on chamber interiors, to run OpenFOAM simulations in parallel, and visualize numerical results using ParaView for in-depth analysis [15,16].

2. Simulations

2.1. Governing equations

A brief summary of governing equations is as follows. As noted above, interFoam is a solver for two incompressible, isothermal, immiscible fluid, which uses the volume of fluid (VOF) phase fraction. Throughout this paper, type write font is used to distinctly indicate reserved keywords by OpenFOAM.

The continuity and phase-fraction transport equations are as follows:

$$\nabla \cdot U = 0 \quad (1)$$

and

$$\frac{\partial \alpha_1}{\partial t} + \nabla \cdot (U \alpha_1) = 0 \quad (2)$$

respectively, and the momentum equation is:

$$\frac{\partial (\rho U)}{\partial t} + \nabla \cdot (\rho U U) = -\nabla p + \nabla \cdot T + \rho f_b \quad (3)$$

where α_1 is the phase-fraction of water, ranging from 0.0 to 1.0. In Eq. (3), T is the stress tensor, and f_b is a body force term including gravity and surface tension, and the fluid density ρ and viscosity μ are estimated as follows:

$$\rho = \alpha_1 \rho_1 + (1 - \alpha_1) \rho_0 \quad (4)$$

$$\mu = \alpha_1 \mu_1 + (1 - \alpha_1) \mu_0 \quad (5)$$

where the subscripts 1 and 0 indicate water and air phases, respectively. More details of the solver can be found elsewhere [17,18].

2.2. Manhole structure and meshing

Fig. 1 shows the cross-sectional view of the inspection chamber of our interest. The representative chamber volume is internally occupied by water and air, as it is surrounded by solid wall surfaces. The top surface is open to the atmosphere. (See section 2.3. for details.) Inlet pipe of a diameter of $D_i = 16$ in (0.406 m) is connected at the left bottom of the chamber, and outlet pipe of diameter $D_o = 18$ in (0.457 m) is located on the right side of the chamber, elevated as high as D_i . The chamber has length $L = 8$ ft (2.4 m) in x -direction and width $W = 4$ ft (1.2 m) in z -direction. The height of the chamber is measured

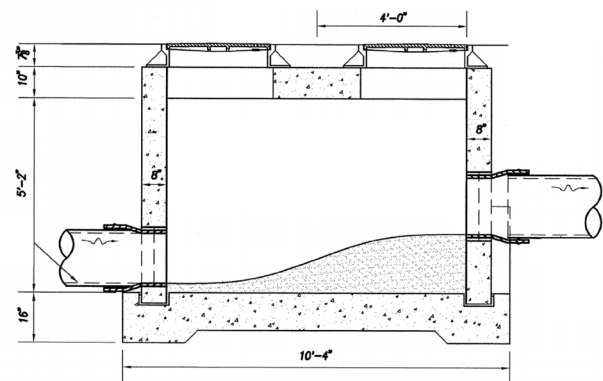


Fig. 1. Section view of a real manhole.

as $H = 6$ ft (1.8 m) from the bottom to the ceiling of the chamber without considering the top solid layer of 10 in (25.4 m). This chamber geometry is summarized in Table 1.

Fig. 2 shows a 3D mesh structure, projected onto $x - y$ plane, which represents the simulation domain, consisting of the water and air phases. For geometrical simplicity and computational efficiency, two circular covers of the chamber, shown in Fig. 1, were removed and the chamber ceiling is made open to the atmosphere. The smooth berm structure shown in Fig. 1 is mimicked as the linear slope, shown in Fig. 2. This approximation is made for simplicity because one of the primary goals of this research is to investigate transient flow patterns and overflow conditions with a constant inflow rate. The original length of the chamber, that is, 8 ft (2.4 m) long, shown in Fig. 1 was elongated to 10 ft (3 m) in Fig. 2 by a new suggested design. We divided the bottom surface into three regions, that is, two flat side regions and a slanted middle berm region. Their horizontal lengths are identically set as $8.0 \text{ ft}/3.0 = 2.67 \text{ ft}$ (0.81 m). The inlet pipe length is set as 16 ft, which is assumed to be long enough to make a fully developed flow field in front of the chamber. An actual distance to the upstream pumping station is much longer than the inlet pipe length, but we assumed that the inlet diameter and inflow rate are more important than the length. The distance between the chamber and the discharging point is 22 ft in a real scale,

which is set equal to the outlet pipe length. The bottom surface of the chamber is perpendicular to the (vertical) gravity direction, and the outlet pipe has 2.4% downward slope to utilize the gravitational force for natural discharge.

We used SolidWorks to make a stereo-lithographic (STL) file of the 3D compound system consisting of a chamber and two pipes. The STL file consisting of several patches (without a volume element) is used to generate a 3D volume enclosed by the patches. We used a default meshing tool of OpenFOAM (version 3.1, obtained from the website <http://openfoam.org>): snappyHexMesh and blockMesh to generate the rectangular meshes shown in Fig. 2. In the x , y , and z directions, the enclosed full volume, having the length of $(16 + 10 + 22)$ ft and the same height and width of the chamber, is divided into 350, 45, and 30 slices in x -, y -, and z - directions, respectively, and mesh points included inside the volume are used for flow simulations. The total number of cells and nodes for simulation are 197,713 and 207,378, respectively, which slightly increase for the larger outlet pipe of 20 and 24 in (0.508 and 0.610 m, respectively). The grid sizes are 1.646, 0.133, and 0.133 in (41.8, 3.4, and 3.4 mm) in x -, y -, and z - directions, respectively. In principle, finer grids may provide simulation results of a higher accuracy, but the unsteady flow simulations may not be able to provide meaningful results within a reasonable amount of time.

Table 1
Chamber and pipe dimensions

	D	L	W	H
Inlet pipe	16.0 in (0.406 m)	16.0 ft (4.9 m)	–	–
Outlet pipe	18.0 in (0.457 m)	22.0 ft (6.7 m)	–	–
Chamber	–	10.0 ft (3.0 m)	4.0 ft (1.2 m)	6.0 ft (1.8 m)

Note: CFD simulations were conducted for three outlet diameters: 18, 20, and 24 in (0.457, 0.508, and 0.610 m, respectively).

2.3. Solution procedure

This section describes the details of our CFD simulations using OpenFOAM. Some reserved keywords in OpenFOAM are written in the typewriter font such as `interFoam` (solver), `zeroGradient`, and `fixedValue`, of which meanings are self-explanatory.

2.3.1. Solver and material properties

OpenFOAM recently became popular in academic and industrial CFD projects. It has more than 80 specific solvers in various physics categories, such as multiphase flow,

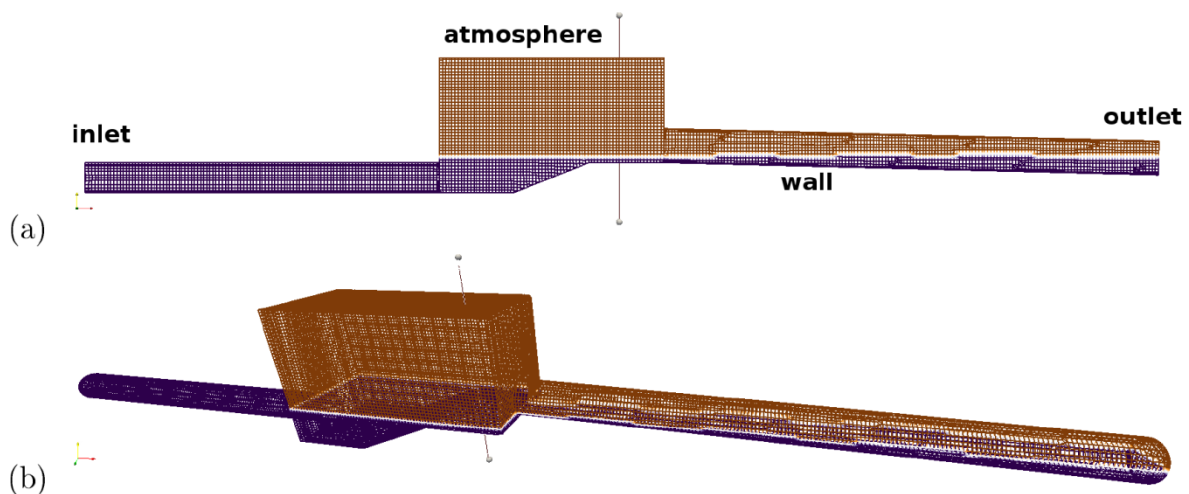


Fig. 2. Generated mesh structures: (a) 2D and (b) 3D views. The lower purple and upper brown regions represent water and air phases, respectively. The vertical line in the y -direction near the chamber outlet indicates a line through which sewage levels are calculated using OpenFOAM simulation results. In addition, x -direction is along the left inlet pipe, and z -direction is out of the $x - y$ plane.

heat and mass transfer, particle tracking, combustion, and so forth. Because the current fluid dynamics problem of the utility chamber has two phases, that is, water and air, we selected interFoam, which solves two isothermal, and immiscible fluids in a transient state. Water fraction denoted here as α_1 determines the liquid and gas phases for $\alpha_1 = 1.0$ and $\alpha_1 = 0.0$, respectively. To calculate α_1 , interFoam uses the interface-capturing approach based on the VOF phase fractions. To capture the turbulent behavior of the sewage flow, we selected RANS equations [4] with $\kappa - \epsilon$ model [19]. Material properties of water and air are listed in Table 2 and used input parameters for interFoam simulations. Both water and air are treated as Newtonian fluids with constant densities and viscosities. The surface tension on the sewage surface is estimated as equal to that between pure water and air at 25°C.

2.3.2. Boundary conditions

For the two-phase simulations, BCs of six variables are determined at four surfaces as summarized in Table 3. These surfaces include wall for all impervious, solid surfaces excluding inlet for the left-most cross section of the inlet pipe, outlet for the right-most cross section of the outlet pipe, and atmosphere for the top, which is an open area. Six physical variables are the net pressure, that is, hydraulic pressure subtracted by the hydrostatic pressure $p - \rho gh$, fluid velocity vector U , water fraction in space α_1 ($0 < \alpha_1 < 1$), turbulent viscosity ν_t , and κ and ϵ in the $\kappa - \epsilon$ model. Specific explanations of the BCs can be found at the OpenFOAM website (<http://openfoam.org>).

Table 2
Properties of water and air used for interFoam simulations

	Water	Air	Unit
Fluid type	Newtonian	Newtonian	–
Density, ρ	998.0	1.21	kg/m ³
Kinematic viscosity, ν	1.0×10^{-6}	1.51×10^{-5}	m ² /s

Note: The surface tension between water and air was set as 0.072 N/m and the gravitational acceleration (9.81m/s²) was used.

Table 3
Boundary conditions on patches and surfaces in OpenFOAM v3.1

	$p - \rho gh$	U	α_1
Wall	fixedFluxPressure	fixedValue	zeroGradient
Inlet	fixedFluxPressure	flowRateInletVelocity	fixedValue
Outlet	pHP	pIOV	zeroGradient
Atmosphere	zeroGradient	zeroGradient	inletOutlet
	κ	ϵ	ν_t
Wall	kqRWallFunction	epsilonWallFunction	nutUWallFunction
Inlet	tIKEI	tMLDRI	calculated
Outlet	zeroGradient	zeroGradient	calculated
Atmosphere	zeroGradient	zeroGradient	calculated

Note: The boundary values of water volume fraction α_1 are 1.0 and 0.0 at inlet and atmosphere boundaries, respectively, and the turbulent viscosity ν_t has the same boundary condition of κ and ϵ on wall boundaries. Some acronyms for long boundary condition names are listed in Symbols section.

2.3.2.1. $p - \rho gh$ The net pressure $p - \rho gh$ has fixedFluxPressure BC on wall and inlet surfaces. This BC adjusts the pressure gradient if the flux on the boundary is specified by velocity BCs, and body forces (such as gravity and surface tension) are present in the governing equations. On the outlet boundary, a typical exit BC can be applied such as zeroGradient, but instead we used an advanced BC, phase-HydrostaticPressure, which fixes pressure if water is present and behaves similarly to zeroGradient when the air is present at the outlet. On atmosphere boundary, the net pressure is set to be zeroGradient as this boundary is considered as an exit cross section.

2.3.2.2. U No-slip BC is used for the flow vector to have a fixedValue of $U = (0, 0, 0)$ on wall boundary. flowRateInletVelocity BC is applied to inlet boundary because it determines a velocity BC, using the (input) volumetric flow rate Q_{in} . Values of the inflow rate Q_{in} of interest are 4, 6, 8, and 9.1 million gallons per day (MGD) (0.175, 0.263, 0.351, and 0.399 cubic meters per second [m³/s], respectively). pressureInletOutletVelocity BC is applied to outlet boundary, where the net pressure value is specified during calculations. This BC is equivalent to zeroGradient for outflow, that is, the flow direction is directed to outward from the fluid volume, and for inflow, the flow velocity is obtained as the normal component of U on the patch surface. Similar to the net pressure, zeroGradient BC is applied as an exit condition for the flow vector. In this study, the surface roughnesses of the pipes and chamber walls are not considered specifically because the inflow rate is preset as a BC and water level inside the chamber has an open interface with air. In open channel hydraulics, the roughness and slope determine a fluid velocity, which is in our study BC.

2.3.2.3. α_1 The water fraction α_1 has simpler BCs as compared with those for the net pressure and flow vector. As the constant inlet flow is assumed, fixedValue ($\alpha_1 = 1$) is assigned on the inlet boundary. zeroGradient BC is applied to wall and outlet boundaries, which indicates imperviousness of solid surfaces and exiting air condition, respectively. On atmosphere boundary, inletOutlet BC is applied to pro-

vide a generic outflow condition. If there is a reverse air flow (to the chamber interior), then α_1 is immediately replaced by zero to prevent any mass flux into the chamber.

2.3.2.4. κ On wall boundary, parameter κ follows `kqRWallFunction`, which enforces `zeroGradient` condition. On inlet boundary, `tKEI` is applied to provide a turbulent kinetic energy condition, based on user-supplied turbulence intensity of $\kappa = 0.05$ (defined as a fraction of the mean velocity). On both outlet and atmosphere boundaries, `zeroGradient` is used for κ , which mimics general exit BC. (See Symbols section for acronyms of long BC names.)

2.3.2.5. ϵ On the wall boundary, parameter ϵ uses `epsilonWallFunction` BC, which determines a turbulence dissipation rate on a solid wall. On the inlet boundary, `tMLDRI` is applied to provide an inlet condition of turbulence dissipation based on a specified mixing length, used in this study as $\epsilon = 1.0 \times 10^{-3}$ m. On both outlet and atmosphere boundaries, `zeroGradient` is used for ϵ , which also mimics general exit BC, similar to κ .

2.3.2.6. ν_t `nutUWallFunction` is used on the wall boundary to provide a turbulent kinematic viscosity ν_t , which is calculated on all other boundaries.

2.3.3. Initial conditions

At $t = 0$, the IC predetermines the transient behaviors of water and air since it is before the fluid flows are fully developed or stabilized. However, using extensively educated values inside the chamber may restrict possible scenarios, which cannot be easily understood without sophisticated CFD simulations.

2.4. Simulation runs: serial and parallel

2.4.1. Serial and parallel runs

A serial run indicates a stand-alone execution of the solver with specified inputs, conditions, and parameters, listed above. Since `interFoam` is a transient solver, the time interval Δt must be specified. A large Δt may reduce simulation runtime, but accumulated error can unexpectedly increase. This error propagation can cause numerical divergence and fail to provide physically meaningful numbers. OpenFOAM has a specific feature to optimize the performance of transient solvers by adjusting Δt (s) with a pre-specified maximum value. Keeping the numerical error below a tolerable error, we used `adjustableRunTime` method to automatically adjust the time step Δt . The numerical stability of OpenFOAM simulation at a local node can be estimated using Courant number, defined as follows:

$$C_0 = \frac{|U|\Delta t}{\Delta x} \quad (6)$$

where $|U|$ is the magnitude of the velocity through a cell of size Δx in the velocity direction. For temporal accuracy and

numerical stability, a Courant number should be maintained below 1.0. We set both the maximum Δt and C_0 below 0.5.

The serial simulations can be optimally run, if the time interval is efficiently adjusted, while keeping the accuracy. For 3D problems, a large number of computational nodes and cells enormously increase the computational runtime. The current work has about 200,000 cells and nodes. Another way to accelerate OpenFOAM is running simulations in parallel, using many computational cores. OpenFOAM has several distinct parallel algorithms depending on how to divide (i.e., decompose) the domain spaces. These are simple, hierarchical, manual, and Scotch.

Simple decomposition requires three division numbers for x , y , and z directions, that is, (n_x, n_y, n_z) . If $(n_x, n_y, n_z) = (4, 2, 2)$, then the computational domain is split into four slices in x direction, and two slices in y and z directions. Hierarchical decomposition requires a sequence of decomposition in addition to the simple decomposition. Scotch decomposition attempts to minimize the number of processor boundaries without requiring geometric inputs from the user (unlike simple and hierarchical decomposition).

As most CFD simulations deal with fluid flows in complex geometries, minimizing inter-processor communication is a primary issue in parallel CFD runs. The performance of simple decomposition sensitively depends on the number of domain slices in each direction, having a fixed total number of computational cores. An optimal set of (n_x, n_y, n_z) for faster performances can be found using the trial-and-error method. On the other hand, scotch decomposition often provides better performance and stability than other two decomposition algorithms with better flexibility of the number of cores. In our parallel OpenFOAM simulations, we used 64 processors (cores) under scotch decomposition algorithm for most parallel simulations.

2.4.2. Run times and domain decomposition

All of the OpenFOAM CFD simulations were conducted using supercomputers, that is, UH HPC2, located at UH Cyber-Infrastructure at the University of Hawaii, Manoa, and Stampede at Texas Advanced Computing Center, Austin, Texas, USA. We used 16 cores of UH HPC2 primarily for developing and testing, and 64 cores of stampede for full-scale simulations. These cores are simultaneously used to run OpenFOAM simulation in parallel. Due to the local flow regimes and overflow conditions, it was hard to compare run times of serial and parallel computations of the two super-computing systems. In each system, a serial run for a case usually takes 2–4 d depending on flow conditions so that without using multi-cores simultaneously it is almost impossible to solve for flows in the chamber. Our estimation indicates that a parallel time evolution for (real) time 1 s requires about 8 min and 30 s using 64 cores in stampede. This estimates the serial runtime using only one of the same cores is 543.8 h (i.e., more than 3 weeks). Without the parallel computation, CFD results cannot be obtained in a reasonable amount of time.

Fig. 3 shows two serial pieces of decomposed sub-domains. The two sub-domains are parts of the outlet pipe, consecutively connected in the x -direction. Using 64 processors, of which identification number ranges from 0 to 63, the full domain of Fig. 2 is decomposed

into 64 sub-domains of smaller volumes. For example, OpenFOAM computation for the two sub-domains is conducted by processor 52 and 53 among 64 processors. The x -ranges of Figs. 3(a) and (b) are from 8.9 to 9.3 and 9.3 to 9.7, respectively, and ranges in y - and z - directions in Fig. 3 are equal to each other. Connectivity of the two sub-domains is clearly shown by the common mesh lines and α_1 values (represented in color plots) at the interfaces. As indicated above, we used scotch parallel algorithm to minimize common interface areas between two consecutive cores because the inter-core communication primarily depends on the area of shared interfaces between two cores and the amount of communicated data.

2.4.3. Visualization using ParaView

We universally used ParaView to visualize the transient behavior of water/air flows and water level, pressure distribution profile, and streamlines [15,16]. Snapshots at important moments were taken, and animation movies were made to investigate fluid dynamic behavior inside the utility chamber. These snapshots are used to discuss transient and steady responses of the sewage flow inside the chamber with given inflow rates and output diameters.

3. Results and discussions

3.1. Effect of outlet diameter D_o in a low inflow rate (4.0 MGD, 0.18 m³/s)

We investigate the flow behavior varying with inflow rate Q_{in} inside the chamber of an outlet diameter D_o . Table 4 shows a total of six combinations of D_o and Q_{in} values as input parameters, and as simulation results, time to reach steady state t_{ss} and the time of t_{of} the first overflow occurrence.

Fig. 4 shows a sewage level in steady state inside the chamber having the outlet pipe of $D_o =$ (a) 18, (b) 20, and (c) 24 in. The initial sewage and air phases are shown in Fig. 2 using purple and brown, respectively. Table 4 indicates the time to reach a steady state and the height, that is, final sewage level on the outlet pipe diameter. We observed that in case A18 the sewage level increases from the chamber bottom to the top-vicinity of the outlet pipe, named in this study as exit-top, within approximately 44 s. Afterward the sewage level barely changes with time. The distance to the exit-top from the bottom surface is the sum of inlet and outlet diameters for cases A18 and B18, that is, 16.0 + 18.0 = 34.0 in. Since the peak sewage level is gradually reached, it is hard

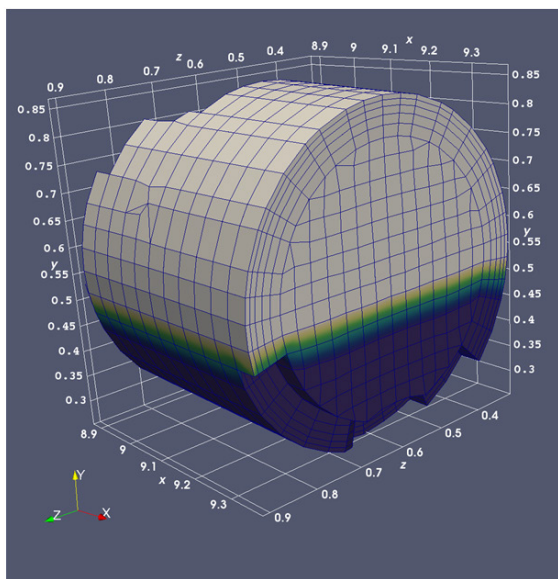
Table 4

Simulation cases A and B have the inflow rate 4 and 8 MGD (0.18 and 0.36 m³/s), respectively, and the following number indicates the outlet diameter in inches

Case	Q_{in}	D_o	t_{ss} (s)	h_{ss} (m)	t_{sm} (s)
A18	4.0 MGD (0.18 m ³ /s)	18.0 in (0.457 m)	44.0	0.78	∞
A20	4.0 MGD (0.18 m ³ /s)	20.0 in (0.508 m)	36.0	0.74	∞
A24	4.0 MGD (0.18 m ³ /s)	24.0 in (0.610 m)	27.0	0.70	∞
B18	8.0 MGD (0.36 m ³ /s)	18.0 in (0.457 m)	–	–	24.0
B20	8.0 MGD (0.36 m ³ /s)	20.0 in (0.508 m)	–	–	115.0
B24	8.0 MGD (0.36 m ³ /s)	24.0 in (0.610 m)	–	–	120.0

Note: Overflow occurs only in B18 case around 40 s.

(a)



(b)

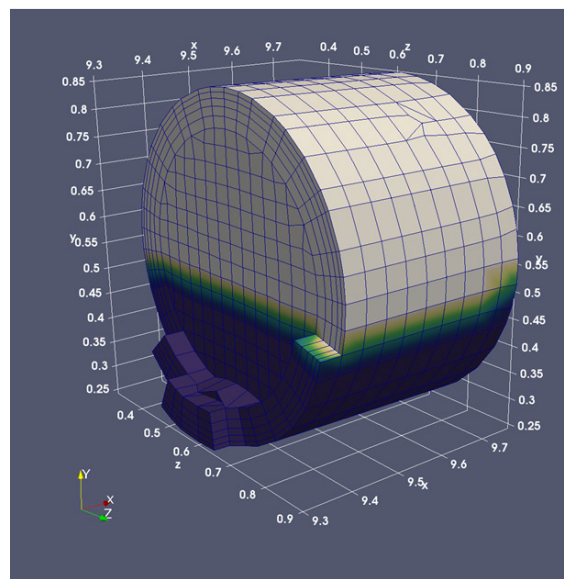


Fig. 3. Decomposed computational sub-domain, assigned to (a) processor-52 and (b) processor-53 among 64 processors (from the identification number from 0 to 63).

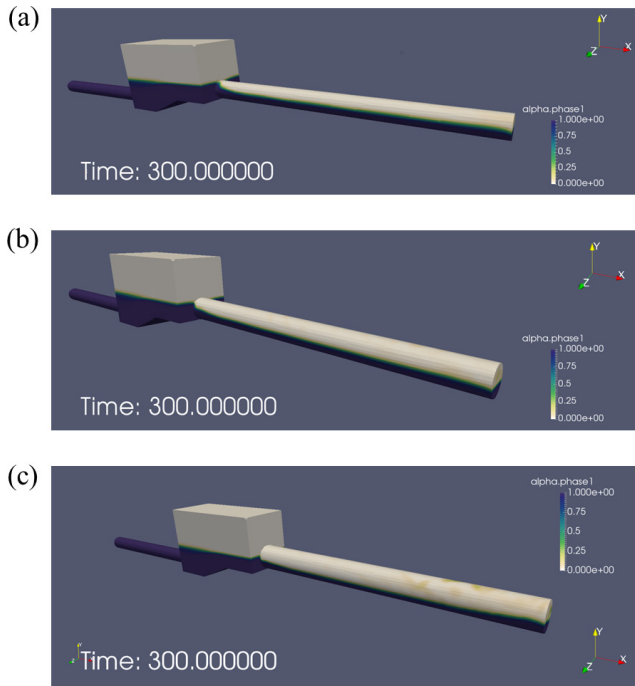


Fig. 4. Final (steady) states of sewage level with the inflow rate $Q_{in} = 4$ MGD ($0.18 \text{ m}^3/\text{s}$) into a chamber of $D_i = 16$ in (0.406 m), $L = 10$ ft (3.0 m), and the outlet diameter of (a) 18.0 (case A18), (b) 20.0 (case A20), and (c) 24.0 (case A24) in (0.457 , 0.508 , and 0.610 m , respectively).

to accurately estimate the elapsed time to reach a steady state t_{ss} . Nevertheless, we visually estimated t_{ss} using flow animations, generated using ParaView. To avoid unnecessary calculations, we set our simulations to automatically (or manually) stop after 300 s in real time. We believe this is long enough for the chamber system to reach a steady state at a low inflow rate or to brim over in a high inflow rate. For the other two cases of A20 and A24, shorter times are required to reach steady states, that is, 36 and 27 s, respectively, and the steady-state sewage level decreases from 0.74 (of A20) to 0.70 m (of A24).

Fig. 5 shows α_1 profiles for three outlet diameters, varying with the vertical distance at the center of the upper berm, located at $x = 8$ ft 4 in (2.54 m) and $z = 2$ ft (0.61 m) shown in Fig. 2. All three D_o cases confirm the liquid-only phase, that is, $\alpha_1 = 1.0$, in the bottom region of the chamber. Above the water level, α_1 rapidly decreases and reaches zero, indicating the air-only phase. The thickness for intermediate values of $0.1 < \alpha_1 < 0.9$ seems to be 10–12 cm, which indicates a humid region for transition between liquid (sewage) and gas (air) phases. Figs. 4 and 5 clearly indicate the following points. For a low inflow rate of 4.0 MGD, the chamber of a larger D_o reaches a steady state in a shorter time with a lower sewage level. This is because as the outlet diameter increases, exiting flow rate of the sewage has a larger cross-section area so that the sewage level must be maintained lower. We observed simple but fundamental facts in this section. An elapsed time to reach a steady state varies with the outlet pipe diameter. Until a steady state is reached, the sewage level does not exceed the exit-top, and flow fields are therefore similar to the open-channel flows.

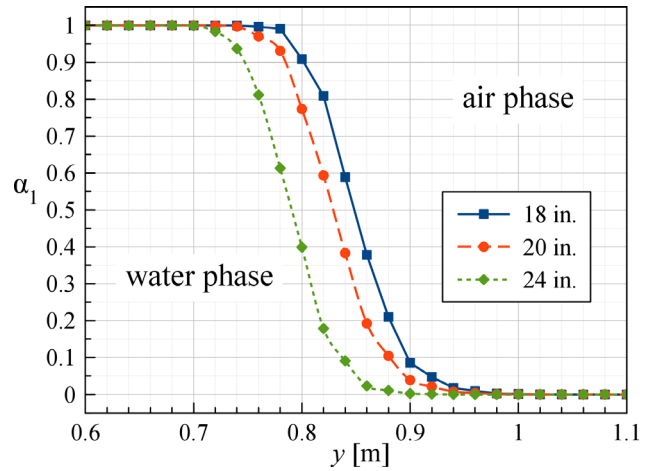


Fig. 5. Sewage levels with 4.0 MGD ($0.18 \text{ m}^3/\text{s}$) inflow rate, measured at the center of the upper berm at a distance 8 ft 4 in (2.54 m) from the inlet wall of the chamber, with respect to the outlet diameter D_o of 18, 20, and 24 in (0.457 , 0.508 , and 0.610 m , respectively).

3.2. Transient behavior in a high inflow rate (8.0 MGD , $0.36 \text{ m}^3/\text{s}$)

Fig. 6 shows transient changes of sewage level in the inspection chamber having an identical geometry to that of Fig. 4. The inflow rate increases from 4.0 to 8.0 MGD (0.18 to $0.36 \text{ m}^3/\text{s}$). The doubled amount of entering water per unit time accelerates the sewage level rise at a much earlier time than that of Fig. 4(a). In case B18, the outlet pipe starts being submerged for the first time at $t_{sm} = 24$ s by the sewage. As the sewage level exceeds the exit-top, the air remaining in the outlet pipe is pushed away to the disposal location at the end of the outlet pipe. This flushing temporarily slows down the rising sewage level. Until $t = 38$ s, the 8 MGD ($0.36 \text{ m}^3/\text{s}$) inflow accelerates the sewage level rise toward the chamber ceiling. A pumping station located upstream pressurizes the entering fluid of the sewage to control the inflow rate. The inflow pressure is released to the atmosphere in the chamber, and the outlet flow is only driven by gravity. If the inflow rate is high, gravitation is not enough to drive sewage flow in the outlet pipe, and therefore the sewage level (continuously) increases in the chamber. Beginning at $t = 39$ s and continuing afterward, the boundary line between the air and sewage phases in the outlet pipe moves along the outlet pipe with time. The sewage level reaches the chamber ceiling (of 6 ft [1.83 m] height) from the bottom of the chamber. Based on the inletOutlet condition of α_1 at atmosphere boundary, the CFD simulation in principle cannot provide physically meaningful results if the sewage level exceeds the top surface. Nevertheless, one can predict that the chamber can hold sewage overflow no more than about 40 s with $Q = 8.0 \text{ MGD}$. If the chamber is initially empty (but the inlet pipe is filled with sewage), then this duration before the overflow may increase as much as the time elapsed to fill the chamber space from the bottom to the exit-top (i.e., 34 in).

Identifying a specific time of overflow requires a large amount of computer time since it usually occurs in the time of an order of 10 min except for cases of both fast inflow rate and small outlet diameter. To determine an occurrence

of the overflow one can try to use a steady-state solver included in OpenFOAM. If the steady-state solver diverges as a final state, it implies that the change to have the overflow is very high, otherwise the chamber will reach a steady state. We observed that when the sewage level starts exceeding the exit-top, flow behavior becomes abruptly unstable and the sewage level starts oscillating vertically. Once the sewage level fully exceeds the outlet pipe, it either rapidly increases to the chamber ceiling or gradually reaches a secondary stable state. Therefore, in our opinion, the time of the first submersion, t_{sm} , of the outlet pipe may give us meaningful information. As indicated in Table 4 and Fig. 6, case B18 has $t_{sm} = 24$ s and $t_{of} = 40$ s. This indicates that an overflow will be almost immediate if 8.0 MGD (0.36 m³/s) inflow rate is entering the chamber of 18-in (0.457 m) outlet diameter. Cases of B20 and B24 do not provide specific overflows, as expected from the longer t_{sm} of 115.0 and 120.0 s, respectively, than that of B18 case. To avoid sewage overflow for 8.0 MGD (0.36 m³/s) inflow rate, the outlet diameter should be at least 20 in. Absolute values of t_{ss} and t_{sm} depend on the initial sewage level inside the chamber. However, a duration to fill the chamber as high as the inlet pipe diameter from the bottom, t_{ic} , can be easily calculated as follows $t_{ic} = V_{ic}/Q_{i'}$ where

$$V_{ic} = \frac{1}{2} \times 10\text{ft} \times 4\text{ft} \times 16\text{in.} = 266.67\text{ft}^3 = 7.55\text{m}^3 \quad (7)$$

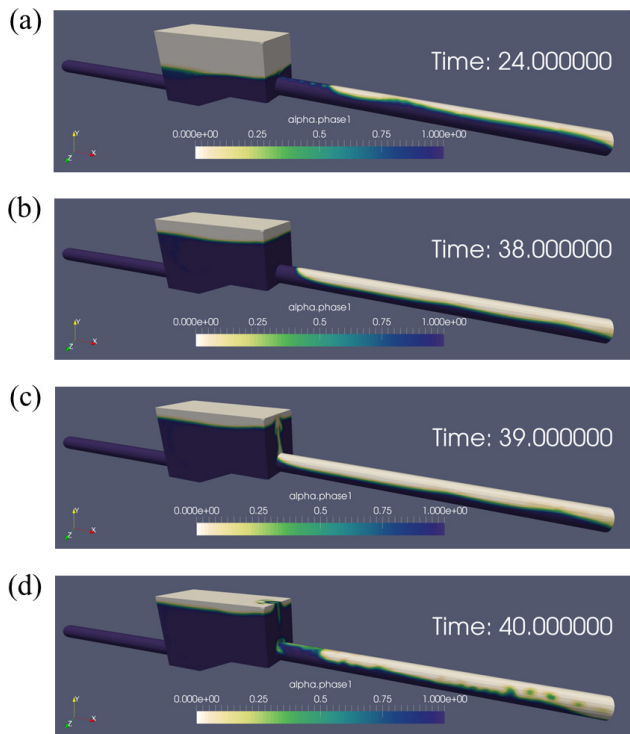


Fig. 6. Transient behavior of sewage level with inflow rate of $Q_{in} = 8$ MGD (0.36 m³/s) for a chamber having $D_o = 18$ in (0.457 m) and $L = 10$ (0.457, 0.508, and 0.610 m, respectively). (These conditions are represented as case B18 in Table 4.) Snapshots are taken at real time at (a) 24, (b) 38, (c) 39, and (d) 40 s using ParaView.

is the liquid volume initially in the chamber. For the inflow rates of 4.0 MGD (=0.17525 m³/s) and 8.0 MGD (=0.350 m³/s), t_{ic} is calculated as 43.08 and 21.57 s, respectively. These short t_{ic} values are in the same order of magnitude of t_{ss} , which confirms its insignificance in this overflow risk assessment. In other words, reaching steady states does not depend on t_{ic} in the low inflow rate cases. Besides, t_{sm} is as short as t_{ic} in the high inflow rate cases if overflow occurs. If the outlet diameter is large enough, then t_{sm} in B-series exceeds 100 s, which is at least five times or more longer than $t_{ic} = 21.54$ s.

3.3. Tantalizing phenomena

3.3.1. 3D investigation

Fig. 7 shows the pseudo-periodic behavior of the sewage level at various times when the level reaches a temporary maximum or minimum along the time line. At 0 s, the sewage level is equal to its IC, shown in Fig. 2. The initial sewage level is as high as the diameter sum of the inlet and outlet pipes, that is, 16 in (0.406 m). From the initial stage, the sewage level monotonously increases until it reaches the first maximum level at 26 s. In the next 11 s after the first peak, the sewage level decreases until it comes below the exit-top, and returns to increasing. This oscillating behavior continues and its time series of the tantalizing trend is visualized in Fig. 8. Once the sewage level exceeds the exit-top, then the space for air transfer between the chamber and the outlet pipe disappears. The hydraulic pressure generating the inflow rate and the atmospheric pressure push the sewage fluid toward the cross-sectional area of the outlet pipe and increase the sewage level. Dynamic accumulation of the sewage fluid in the chamber over the outlet pipe increases the gravitational pressure near the outlet pipe. Consequently, the level goes down and the amount of sewage corresponding to the height difference is flushed out through the output pipe. Overall, we observed an interesting phenomenon related to the steady and tantalizing states as given below:

- First, there are two flow regimes based on how to reach a steady state. At a given inflow rate, the outlet diameter determines the presence of the steady state or vice versa.

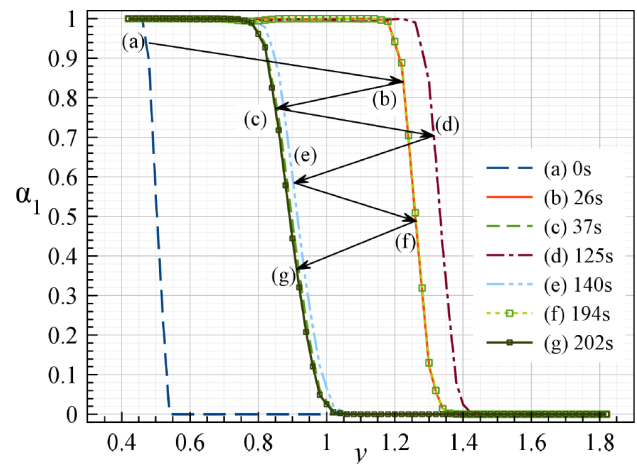


Fig. 7. Tantalizing behavior of sewage level with various times of case B20.

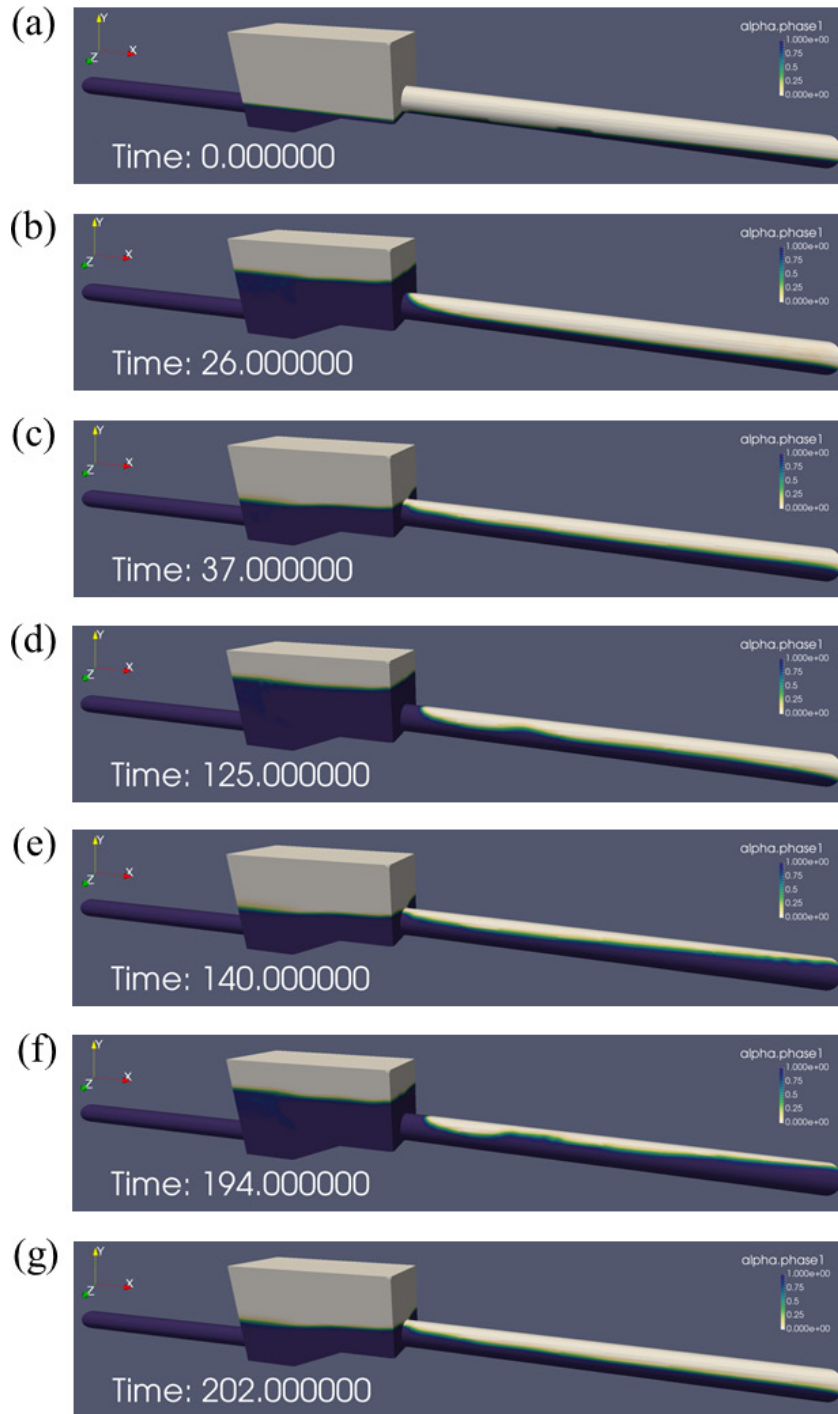


Fig. 8. Alternating maximum and minimum sewage levels at peak times, (a)–(g) corresponding to Fig. 7.

As long as the outlet diameter is large enough so that sewage level does not reach the exit-top of the outlet pipe, a steady state is definitely reached and maintained.

- Second, if the inflow rate is large enough to have the sewage level higher than the exit-top, then a steady state is absent, but an oscillating phase of the sewage level across the exit-top is predominant.
- Third, by carefully observing flow animation, we found an intrinsic flow instability near the exit-top when

the sewage level tries to exceed it. This tantalizing phenomenon implies that the absence of a steady state is fully determined by the chamber structure.

3.3.2. 2D investigation

Fig. 9 shows a transient variation of the physical variables measured at various times from the initial state. The background color (indicating the net pressure, $p - \rho gh$) is shown

with 50% of transparency, so that the presence of the inlet and outlet pipes is shown as two circular regions, where the upper outlet pipe is slightly larger than the lower inlet pipe because their diameters are 18 and 16 in (0.457 and 0.406 m), respectively. Hydraulic phenomena are explained as follows:

a. Initially at $t = 1.0$ s, the sewage level shows a plateau shape with little fluctuation on the liquid surface. Arrows in the bottom circle of the inlet pipe are directed out of the paper. The net pressure ($p - \rho gh$) below the sewage level is, as expected, much higher than that of the air phase.

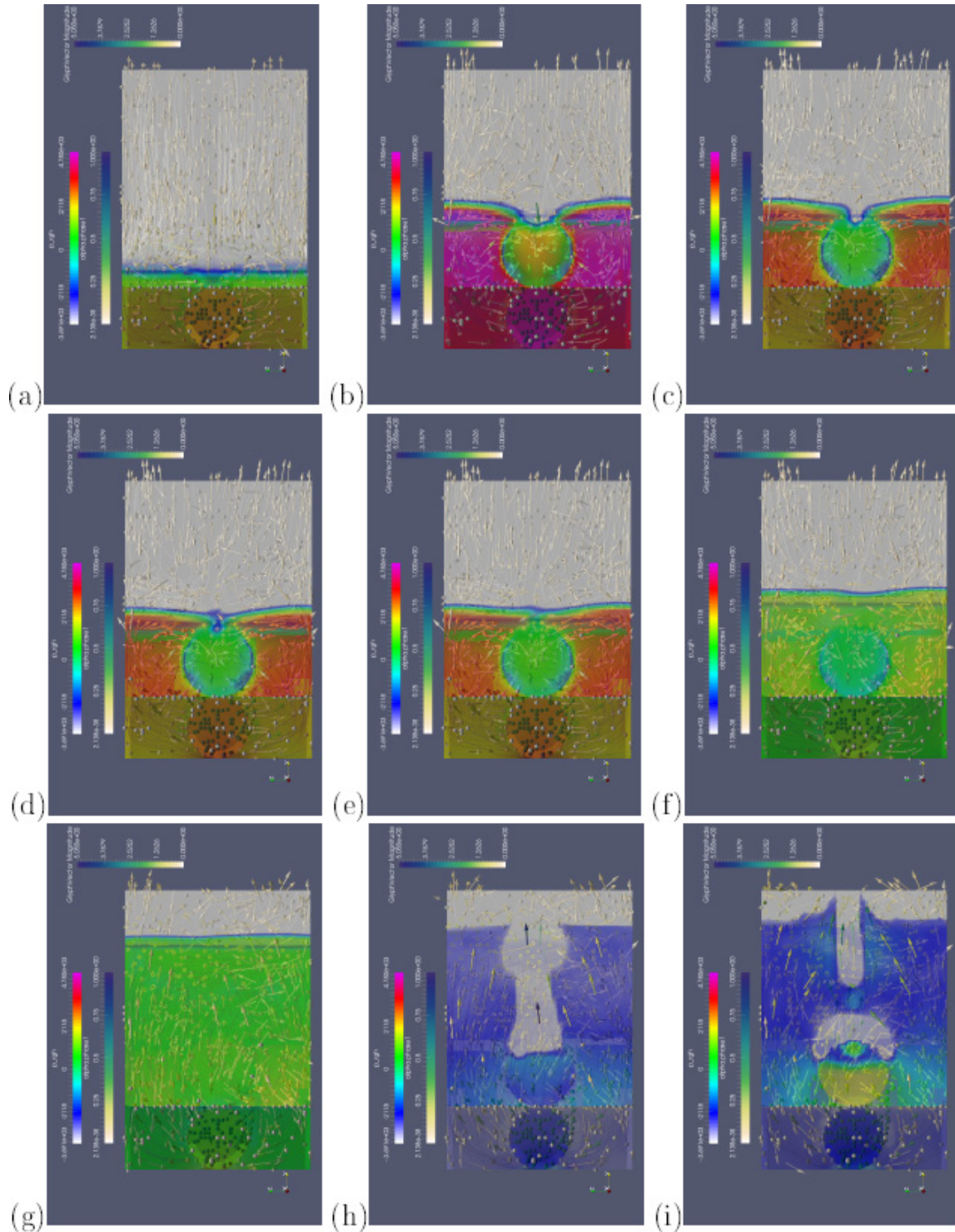


Fig. 9. Snapshots of B18 case from outlet to inlet side in front of the flow exit plane at time (a) 1, (b) 12, (c) 20, (d) 22, (e) 24, (f) 30, (g) 38, (h) 39, and (i) 40 s. Colors of the background, arrows, and streamlines indicate values of $p - \rho gh$, flow speed U , and liquid fraction α_l , respectively.

- b. Since the inflow rate is high, that is, 8.0 MGD ($0.36 \text{ m}^3/\text{s}$), the sewage level increases promptly within 12 s. The sewage level on the side walls is higher than that of the exit-top while the outlet pipe is not completely submerged. The background color besides the outlet pipe shows the highest pressure before an overflow occurs later.
- c. Interestingly, as the small area through which air can pass near the exit-top decreases with time, the hydraulic pressure applied on the cross section of the outlet pipe becomes less. At time $t = 20$ s, flow filled on the left- and right-hand sides of the outlet pipe rotate in the clockwise and counter-clockwise directions, respectively. It is because the flow in the outlet pipe is similar to the open-channel flow. Fluid elements near the sewage-level experience less hydraulic drag than those near the pipe wall. If the entire outlet pipe is submerged, then the flow inside the outlet pipe is close to simple pipe flow. As the output pipe has an oscillating sewage level, the anisotropic secondary turbulence did not appear [20]. The net pressure built below the sewage level decreases and becomes less than that in (b).
- d. At $t = 22$ s, the sewage level returns almost flat, and the air-passing region is much smaller than those at time $t = 12$ and 20 s. From this time, the air zone is trapped in the entering region of the outlet pipe. It is because the sewage level starts exceeding the exit-top.
- e. The air zone disappears at $t = 24$ s as it is flushed downstream along with the sewage flow. Variation of the air fraction along the output pipe in the x -direction is shown in Fig. 6(a). As the trapped air is pushed away from the chamber, it is not clearly shown in this 2D projection. This quick flushing may lead to the gradual decrease in the net pressure built below the sewage level.
- f. Passing time $t = 30$ s, the sewage level continuously increases above the exit-top. The flow field inside the chamber seems to reach a temporarily stable state. During this short period, the sewage level is maintained flat similar to that of (a), and the surface water line has a similar shape as Fig. 9(d).
- g. Near $t = 30$ s, the sewage level is above the exit-top, and the outlet flow does not effectively reduce the rise of the sewage level. The tantalizing phenomena start at time $t = 12$ s, and until now it takes only 26 s (near an overflow). It is, therefore, clear that an 18-in (0.457 m) outlet pipe holds the fast inflow rate of 8.0 MGD ($0.36 \text{ m}^3/\text{s}$) only shortly because the overflow will occur within a minute. From the time that the tantalizing phenomenon starts at $t = 12$ s to the time that the sewage level reaches its temporary maximum around $t = 38$ s, it took only 26 s. Therefore, it is clear that an 18-in (0.457 m) outlet pipe cannot hold the inflow rate of 8.0 MGD ($0.36 \text{ m}^3/\text{s}$) long enough since the overflow will be almost instantaneous, that is, within a minute.
- h. A high sewage level (close to the ceiling) accumulates the gravitational pressure and hence initiates the abrupt flushing at time $t = 39$ s. The gravity-driven sewage flushing generates a large air pocket. The net hydraulic pressure suddenly decreases as the blue-tone color indicates. The large air pocket in the chamber also creates a small air pocket near the exit-top, which is enhanced by the backdraft of air in the reverse direction of the outflow along the outlet pipe.
- i. At $t = 40$ s, the large air pocket is split into two parts, which must be due to the recovering flow in the lateral direction. Air in the top portion of the pocket of (h) blows up toward the atmosphere and air in the bottom of the pocket is flushed downstream. In principle, the accuracy of our interFoam simulation is not entirely guaranteed from this moment when the liquid phase touches the ceiling. Nevertheless, one can indicate that the tantalizing phenomena occur almost immediately, followed by an overflow within a minute.

3.4. Result verification and convergence test

In this section, we provide a backward check and implicitly validate our results shown above. First, we assumed in the initial state that the inlet flow is fully developed along the inlet pipe, having the BC of the fixed flow rate at the inlet (Table 4). The flow speed ranges from 1.40 to 3.17 m/s as calculated using the inflow rates and the cross-sectional area of the 16-in (0.406 m) inlet pipe. Fig. 10 shows the three velocity components, measured in the middle of the inlet pipe along the vertical (y -) direction. The flow conditions indicate that this flow is in the steady turbulent regime. The velocity component along the inlet pipe, U_x , is dominant as compared with those of other directions, that is, U_y and U_z . The U_x profile is not parabolic, but almost of plateau except near the pipe surfaces, where the vertical line of $y = 0.2032$ m indicates the central line of the inlet pipe. The Reynolds number of the inlet pipe flow is of an order of $O(10^5)$, which indicates that the flow is in a turbulent regime. This also explains the plateau flow-profile shown in Fig. 10 with the range of the Reynolds number. Fig. 11 shows average and maximum (bulk) Courant numbers and their interface values (at surfaces) with respect to the real time for investigation. The interface Courant number only deals with the velocity of the interface normal to itself in surface cells. In our simulations, the maximum Courant number was preset as 0.5. At any instance during the simulation, if the (bulk) Courant number exceeds its maximum value, the time step Δt is adjusted (shortened) to reduce the Courant numbers. As shown in Fig. 11, the (bulk)

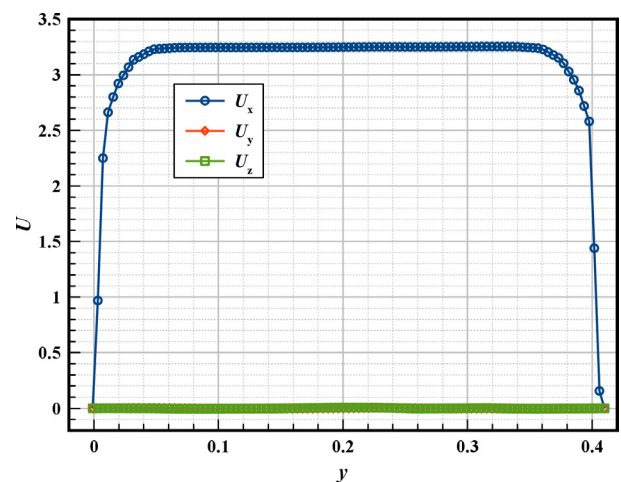


Fig. 10. Profiles of velocity components along the y -direction in the middle of the inlet pipe using $Q_{\text{in}} = 9.1$ MGD ($0.40 \text{ m}^3/\text{s}$) and $D_o = 24$ in (0.610 m).

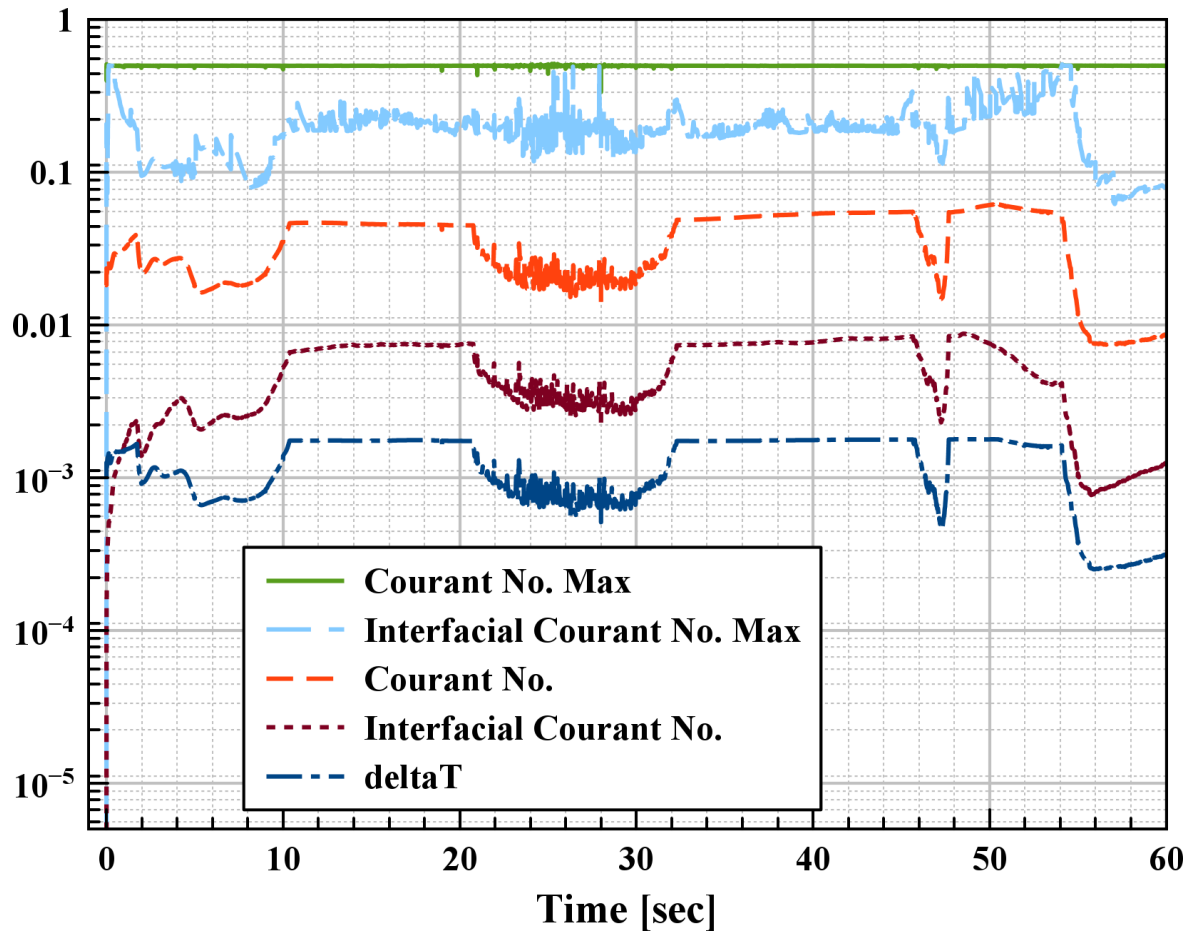


Fig. 11. Converging analysis using $Q_{in} = 9.1$ MGD ($0.40 \text{ m}^3/\text{s}$) and $D_o = 24$ in (0.610 m).

Courant number was maintained near 0.01, that is, one order of magnitude smaller than the preset maximum, by having the adjusted time step of an order of $O(10^{-3})$ s. The maximum interface Courant number also does not exceed 0.5.

4. Conclusions

In order to maintain urban infrastructure and sustainability, storm runoff needs to be efficiently drained through underground sewer systems. As an overflow, that is, spillover, of a utility chamber causes a variety of hydraulic problems in urban life, scientific design of a utility chamber is of great necessity to hold a large amount of sewage flow for a short period. In this light, we conducted CFD simulations of OpenFOAM for two-phase flow inside a chamber, connected to inlet and outlet pipes. For a slow inflow rate, that is, 4 MGD ($0.18 \text{ m}^3/\text{s}$), the outlet pipe is not submerged so that a steady state is quickly reached. The chamber consisting of a larger outlet diameter reaches the steady state (much) faster having a lower sewage level. For a fast inflow rate, for example, 8 MGD ($0.36 \text{ m}^3/\text{s}$), the sewage level continuously changes and periodically fluctuates with time. Although temporary meta-stable states are visually observed, the quasi-stability does not last long. The tantalizing phenomenon is continuously observed that the sewage level is continuously moving up and down,

eventually passing the top level of the outlet pipe. A steady state, therefore, does not exist if the inflow rate is fast enough. In our opinion, the junction interface between the chamber and the outlet pipe plays a critically important role in stabilizing flow fields inside the chamber. This is because the tantalizing effect spatially originates at the exit-top. Parallel computation of OpenFOAM, that is, interFoam solver in our case, is proven to be reliable and efficient as it provides physically consistent results within a reasonable amount of time. An advanced design of the chamber interior with a small structural change can potentially prevent the chances of spillover or reverse flow of sewage in underground sewer systems.

Acknowledgments

This research used the Extreme Science and Engineering Discovery Environment (XSEDE), which is supported by National Science Foundation grant number ACI-1053575, and was financially supported by R.M. Towill Corporation, Honolulu, Hawaii, USA. The authors appreciate Mr. Jonathan Imai for his SolidWorks drawing for the mesh generation. This work was also supported by The Kohala Center of the Hawaiian Scholars Doctoral Fellowship Program, The Deviants from the Norm Fund and Dr. Paul and Elizabeth Nakayama for the second author.

Symbols

pHP	—	phaseHydrostaticPressure
pIOV	—	pressureInletOutletVelocity
tIKEI	—	turbulentIntensityKineticEnergyInlet
tMLDRI	—	turbulentMixingLengthDissipationRateInlet

Greek

ν	—	Kinematic viscosity
ν_t	—	Turbulent kinematic viscosity
ρ	—	Density

Subscripts/Superscripts

0	—	Air phase
1	—	Water phase
b	—	Body
ic	—	Inside the chamber

Mathematical symbols

U	—	Flow vector
D_i	—	Inlet diameter
D_o	—	Outlet diameter
H	—	Chamber height
h_{ss}	—	Sewage level in a steady state
L	—	Chamber length
n_x, n_y, n_z	—	Mesh division numbers in x , y , and z directions, respectively
p	—	Pressure
Q_{in}	—	Inflow rate, MGD or tons/s
t_{sm}	—	Time occurring the first submerging of outlet pipe
t_{ss}	—	Time to reach a steady state
U	—	Flow speed
W	—	Chamber width

References

- [1] E. Iatan, M. Iliescu, F. Bode, I. Nastase, R.M. Damian, M. Sandu, Numerical study for open-channel flow over rows of hemispheres, *Energy Procedia*, 85 (2016) 260–265.
- [2] F.R. Menter, Two-equation eddy-viscosity turbulence models for engineering applications, *AIAA J.*, 32 (1994) 1598–1605.
- [3] S. Edwini-Bonsu, P.M. Steffler, Air flow in sanitary sewer conduits due to wastewater drag: a computational fluid dynamics approach, *J. Environ. Eng. Sci.*, 3 (2004) 331–342.
- [4] G. Alfonsi, Reynolds-averaged Navier–Stokes equations for turbulence modeling, *Appl. Mech. Rev.*, 62 (2009) 040802.
- [5] I. Galambos, Improved Understanding of Performance of Local Controls Linking the above and below Ground Components of Urban Flood Flows, PhD Thesis, University of Exeter, Exeter, UK, 2012.
- [6] S. Djordjević, A.J. Saul, G.R. Tabor, J. Blanksby, I. Galambos, N. Sabtu, G. Sailor, Experimental and numerical investigation of interactions between above and below ground drainage systems, *Water Sci. Technol.*, 67 (2012) 535–542.
- [7] J. Leandro, P. Lopes, R. Carvalho, P. Páscoa, R. Martins, M. Romagnoli, Numerical and experimental characterization of the 2D vertical average-velocity plane at the center-profile and qualitative air entrainment inside a gully for drainage and reverse flow, *Comput. Fluids*, 102 (2014) 52–61.
- [8] S. Lau, V. Stovin, I. Guymer, Scaling the solute transport characteristics of a surcharged manhole, *Urban Water J.*, 5 (2008) 33–42.
- [9] M.P. Allen, D.J. Tildesley, *Computer Simulation of Liquids*, Clarendon Press, New York, NY, USA, 1987.
- [10] M. Balogh, A. Parente, C. Benocci, RANS simulation of ABL flow over complex terrains applying an enhanced k- ϵ model and wall function formulation: implementation and comparison for fluent and OpenFOAM, *J. Wind Eng. Ind. Aerodyn.*, 104–106 (2012) 360–368.
- [11] F. Greifzu, C. Kratzsch, T. Forgber, F. Lindner, R. Schwarze, Assessment of particle-tracking models for dispersed particle-laden flows implemented in OpenFOAM and ANSYS FLUENT, *Eng. Appl. Comp. Fluid Mech.*, 10 (2016) 30–43.
- [12] P.K. Kang, W.H. Lee, S.H. Lee, A.S. Kim, Origin of structural parameter inconsistency in forward osmosis models: a pore-scale CFD study, *Desalination*, 421 (2017) 47–60.
- [13] A.S. Kim, S.J. Ki, H.-J. Kim, Research perspective of membrane distillation: multi-scale and multi-physics phenomena, *Desal. Wat. Treat.*, 58 (2017) 351–359.
- [14] A.S. Kim, M.S. Park, J.H. Min, Computational fluid dynamics simulation of Liqui-Cel membrane using OpenFOAM: implication for membrane distillation, *Desal. Wat. Treat.*, 58 (2017) 360–367.
- [15] J. Ahrens, B. Geveci, C. Law, *ParaView: An End-User Tool for Large Data Visualization*, Visualization Handbook, Elsevier, Amsterdam, Netherlands, 2005.
- [16] U. Ayachit, *The ParaView Guide: A Parallel Visualization Application*, Kitware Inc., New York, USA, 2015.
- [17] H.G. Weller, G. Tabor, H. Jasak, C. Fureby, A tensorial approach to computational continuum mechanics using object-oriented techniques, *Comput. Phys.*, 12 (1998) 620–631.
- [18] C.J. Greenshields, *OpenFOAM User Guide version 4.0*, 2016.
- [19] B.E. Launder, D.B. Spalding, The numerical computation of turbulent flows, *Comput. Methods Appl. Mech. Eng.*, 3 (1974) 269–289.
- [20] P. Bradshaw, Turbulent secondary flows, *Annu. Rev. Fluid Mech.*, 19 (1987) 53–74.